

Effect of droplet interaction on droplet-laden turbulent channel flow

J. G. M. Kuerten^{1,a),b)} and A. W. Vreman^{2,c)}

¹*Department of Mechanical Engineering, Eindhoven University of Technology, P.O. Box 513, 5600 MB Eindhoven, The Netherlands*

²*Research Development & Innovation, Process Technology, AkzoNobel, P.O. Box 10, 7400 AA Deventer, The Netherlands*

(Received 27 August 2014; accepted 10 May 2015; published online 22 May 2015)

We present results of direct numerical simulation of heat transfer and droplet concentration in turbulent flow of a mixture of dry air, water vapor, and water droplets in a differentially heated channel. In particular, we study the effects of droplet collisions by comparing results of simulations with and without droplet collision model for several overall droplet volume fractions. The results show that droplet collisions have a large influence on droplet concentration. Maximum local concentrations, which occur close to the walls of the channel, are reduced by almost an order of magnitude for the case with the highest overall volume fraction. In addition, the positive skewness of the local volume fraction is reduced by a factor of two near the walls. These findings show the importance of including four-way coupling, even in cases where the overall droplet volume fraction is only on the order of 10^{-4} and the Stokes number in wall units is only about 10. In spite of this large effect of droplet collisions on droplet concentration, the effect on the overall heat transfer between the walls of the channel is not more than approximately 17%. That the effect on the overall heat transfer is relatively small can be explained by the lower heat exchange area between droplets and gas in the near-wall areas, which results in a higher temperature difference between droplets and surrounding gas. © 2015 AIP Publishing LLC. [<http://dx.doi.org/10.1063/1.4921492>]

I. INTRODUCTION

Recently, it has been shown by means of numerical simulation that the presence of small, heavy particles with high specific heat can significantly increase the heat transfer properties of a differentially heated turbulent channel flow.¹ This increase is caused by the temperature difference between the particles and the continuous phase close to the wall, where the particle concentration is higher than average due to turbophoresis. In a later paper,² it has been shown that the increase in heat transfer can be further augmented if the particles are replaced by droplets which can grow and shrink by phase change when the continuous phase consists of a mixture of dry air and the vapor of the dispersed phase. This further increase in heat transfer can be understood from the larger temperature difference between the two phases caused by the enthalpy of evaporation, which cools the droplets close to the hot wall where evaporation occurs, and heats the droplets close to the cold wall, where condensation of the vapor occurs.

In both papers, the Euler-Lagrange formulation has been applied, where the continuous phase is described by the Eulerian approach and a Lagrangian point-particle approach is used for each droplet or particle.³ This approach is allowed if the particles are smaller than the smallest scales present in the turbulent flow. For the continuous phase, a direct numerical simulation (DNS) has been applied. In order to describe the temperature and vapor mass fraction in the continuous phase,

a) Also at Faculty EEMCS, University of Twente, The Netherlands.

b) Electronic mail: j.g.m.kuerten@tue.nl

c) Electronic mail: bert.vreman@akzonobel.com

apart from the Navier-Stokes equation also convection-diffusion equations for the temperature and vapor mass fraction have been solved. It has been shown⁴ that for the test cases studied by Russo *et al.*,² a compressible and an incompressible formulation for the continuous phase yield very similar results for most quantities of interest. For each droplet apart from the usual equations of motion, equations for its temperature and its mass have been solved, which take into account the convective heat transfer between the two phases, the enthalpy of evaporation when phase change occurs, and the deviation from saturation. The equations have been closed by empirical correlations for the drag force, Nusselt number, and Sherwood number for spherical particles.⁵

In all test cases considered in the paper by Russo *et al.*,² the initial uniform volume fraction of droplets is 2.2×10^{-4} or lower, while the droplet relaxation time is not much larger than the Kolmogorov time throughout the channel. The Stokes number in wall units, St^+ , is nearly equal to 10. Therefore, the simulations are in the regime of two-way coupling according to the criteria proposed by Elghobashi.³ This implies that the continuous phase influences the dispersed phase and vice versa, but direct interaction between two droplets or particles has not been accounted for. However, due to turbophoresis, during the simulation, the droplet concentration becomes non-uniform in the wall-normal direction, reaching values more than a factor of 10 higher than the initial concentration close to the wall. Moreover, the droplets are preferentially located in the low-speed streaks close to the walls. Therefore, locally the droplet concentration may reach even higher values, which might make the disregard of direct interaction between droplets, usually called four-way coupling, questionable.

In this paper, the effect of droplet collisions on the properties of droplet-laden turbulent flow in a differentially heated channel will be studied for the reference test cases considered by Russo *et al.*² In particular, it will be shown how droplet collisions influence the droplet concentration and how this affects the temperature profile of the continuous phase in the steady state.

Numerical simulations of particle-laden flow with two-way and four-way coupling have been reported in a number of papers over the last 20 years. Compared to simulations of particle-laden turbulent flow employing one-way and two-way coupling, simulations with four-way coupling have initially been hampered by the lack of efficient collision detection algorithms. One of the first studies that took into account collisions between finite-sized particles was by Sundaram and Collins⁶ on particle collisions in isotropic turbulence. Compared to the brute-force collision detection algorithm that checks for collisions between all particle pairs, they divided the computational domain into blocks and checked for collisions between particles in the same or a neighboring block. Chen *et al.*^{7,8} were the first to perform DNS of droplet-laden channel flow with four-way coupling. DNS and large-eddy simulation (LES) of gas-solid channel flow with four-way coupling have been performed by Li *et al.*⁹ and by Yamamoto *et al.*¹⁰ Mass loads of the dispersed phase up to a value of 30 in gas-solid turbulent pipe and channel flows have been studied by means of DNS by Vreman¹¹ and by means of LES by Vreman *et al.*¹² This literature shows that for small overall volume fractions, on the order of 1×10^{-4} , the mean particle concentration close to the wall decreases significantly when particle collisions are taken into account for $St^+ = 192$ in DNS of channel flow,⁹ for $St^+ = 27$ in LES of channel flow,¹⁰ and for $St^+ = 85$ in DNS of pipe flow.¹¹ In the present work, we also find large effects of collisions on particle concentration, while St^+ is considerably lower than in the references mentioned. This is relevant, since Elghobashi³ indicates that the boundary between the two-way and four-way coupling regimes shifts toward smaller volume fractions for particles with higher Stokes numbers. In addition, we investigate which impact a reduced mean volume concentration at the wall by particle collisions has on the Nusselt number.

Apart from the collision detection method, the type of collision method plays an important role. A hard-sphere collision model, including particle rotation, in which the collisions are treated in a deterministic way has been developed by Hoomans *et al.*¹³ Such a model, either with or without particle rotation, has been applied by various other authors.^{11,12,14,15} Other methods treat the particle collisions in a stochastic way,^{16,17} but these methods are restricted to high particle number density or almost homogeneous flows.

In this paper, droplet collisions will be treated in a deterministic way with a hard-sphere collision model, in which all droplet-pair collisions are detected. Since we consider small droplets, that can be assumed spherical, and the mass density of the droplets is large compared to the mass density

of the continuous phase, the droplet-laden flow we consider is in most respects very similar to particle-laden flow. The most important difference is the mass transfer between the two phases by means of evaporation of droplets and condensation of vapor, which results in a non-constant droplet diameter. Unlike in the paper by Chen *et al.*,⁷ it will be assumed that droplets do not coalesce when they collide, but perform a fully or non-fully elastic collision. For the small droplets considered in this paper, the Weber number for two colliding droplets, based on their relative velocity and average diameter, is sufficiently small that coalescence of two colliding droplets is unlikely.^{18–20} It will also be assumed that a droplet bounces back if it collides with a wall, which is a valid assumption if the wall is super-hydrophobic.²¹ The droplet-wall collisions will be assumed either elastic or inelastic. In practice, restitution coefficients somewhat smaller than 1 have been observed.²¹

The present paper and the literature cited deal with dilute flows in which the volume fraction of the dispersed flow is lower than approximately 0.01. Note, however, that the Euler-Lagrange approach with deterministic particle collisions has also been applied to much denser flows (see the review papers by van der Hoef *et al.*²² and Deen *et al.*²³ and the references therein).

The organization of this paper is as follows. In Sec. II, the physical model applied in this work will be presented along with the numerical method used to solve the set of equations. Section III shows results for droplet concentration, Sec. IV for collision frequency, whereas Sec. V considers the resulting temperature profile and its consequences for the heat transfer properties. Finally, Sec. VI will present conclusions of this investigation.

II. PHYSICAL MODEL AND NUMERICAL METHODS

Since the physical model and numerical method are the same as those used by Russo *et al.*,² only the most relevant parts will be recalled here. In Subsection II A, the model for the continuous phase will be given, while in Subsection II B, the governing equations for the droplets and in Subsection II C, the numerical methods will be specified. Finally, in Subsection II D, we will give a short overview of the collision algorithm.

A. Continuous phase

The continuous phase is a mixture of dry air and water vapor. It is treated in an Eulerian way and assumed to be incompressible. This implies that the mass densities of the two components, ρ_a of dry air and ρ_v of water vapor, are allowed to vary in time and space, as long as their sum is constant: $\rho_a + \rho_v = \rho_g = \text{const}$, where ρ_g is the mass density of the gas phase. Hence, the gas satisfies the continuity equation for incompressible flow,

$$\nabla \cdot \mathbf{u} = 0, \quad (1)$$

where \mathbf{u} is the velocity of the gas. Moreover, the gas momentum equation is modeled by the Navier-Stokes equation for incompressible flow, supplemented with a model for the interaction force between the two phases,

$$\frac{\partial \mathbf{u}}{\partial t} + \omega \times \mathbf{u} + \nabla P = \nu \Delta \mathbf{u} + \frac{\mathbf{F}}{\rho_g} + \frac{\mathcal{L}_{\mathbf{u}}}{\rho_g}, \quad (2)$$

where $\omega = \nabla \times \mathbf{u}$ is the vorticity, $P = p/\rho_g + \frac{1}{2}\mathbf{u}^2$, ν is the kinematic viscosity of the gas, p the static pressure, and \mathbf{F} is the driving force necessary to maintain a constant total mass flow rate. Finally, $\mathcal{L}_{\mathbf{u}}$ describes the momentum exchange between the two phases that will be specified in Subsection II B.

The vapor mass density changes because of diffusion, convection, and mass transfer between the two phases by evaporation and condensation,

$$\frac{\partial \rho_v}{\partial t} + \nabla \cdot (\rho_v \mathbf{u}) - \nabla \cdot (\mathcal{D} \nabla \rho_v) = \mathcal{L}_v. \quad (3)$$

The term \mathcal{L}_v represents the mass transfer between water droplets and water vapor that will be specified in Subsection II B. We assume that the diffusion coefficient \mathcal{D} is constant in space and

time, which is justified since the vapor concentration is much lower than the concentration of dry air.⁵

The equation for the gas temperature, T_g , follows from conservation of energy. The contribution of kinetic energy to the total energy is very small at the low velocities we consider in this paper, as has been shown by Bukhvostova *et al.*⁴ Therefore, the gas temperature equation can be expressed as

$$(\rho_a c_{v,a} + \rho_v c_{v,v}) \left(\frac{\partial T_g}{\partial t} + \nabla \cdot (\mathbf{u} T_g) \right) = k_g \nabla^2 T_g + \mathcal{L}_{\text{wd}} + \mathcal{L}_{\text{diff}} + \mathcal{L}_{2\text{way}}, \quad (4)$$

where $c_{v,a}$ and $c_{v,v}$ are the specific heat at constant volume of dry air and water vapor, respectively, and k_g is the thermal conductivity. It is assumed that the heat diffusivity $k_g / (\rho_a c_{v,a} + \rho_v c_{v,v})$ in (4) is constant, which is accurate for the small values of the vapor mass fraction considered here.²⁴ The dependence of k_g on ρ_v is taken into account in the term \mathcal{L}_{wd} , which also represents the transport of energy due to diffusion of water vapor,

$$\mathcal{L}_{\text{wd}} = \left\{ \frac{\partial k_g}{\partial \rho_v} + \mathcal{D}(c_{p,v} - c_{p,a}) \right\} \nabla \rho_v \cdot \nabla T_g. \quad (5)$$

The third term on the right-hand side of (4) stems from diffusion of vapor and is equal to²

$$\mathcal{L}_{\text{diff}} = (R_a - R_v) \mathcal{D}(T_g - T_{\ell_0}) \nabla^2 \rho_v, \quad (6)$$

where $R_a = c_{p,a} - c_{v,a}$ and $R_v = c_{p,v} - c_{v,v}$ are the specific gas constants of dry air and vapor and T_{ℓ_0} is the reference temperature where the latent heat is evaluated. Finally, $\mathcal{L}_{2\text{way}}$ represents the contribution from the coupling between the two phases, which will be specified in Subsection II B.

B. Dispersed phase

The dispersed phase consists of water droplets, which are treated in a Lagrangian way, by solving equations for the position, velocity, temperature, and mass of each individual droplet. Furthermore, droplets are so small that a point particle approach is allowed. Droplets are so small that it may be assumed that they are spherical in very good approximation. Even close to the walls of the channel, where the shear rate of the flow is maximum, the typical value of the capillary number is not larger than 10^{-5} and this leads to deformation parameters of the same order of magnitude.²⁵ Since the mass density of a droplet is large compared to the mass density of the gas, the only relevant force between the two phases is the drag force. Moreover, in most of the simulations discussed in this paper, we do not take gravity into account in order to enable a comparison with the results of Russo *et al.*² without droplet collisions. However, in order to study the effect of gravity, we performed one simulation with gravity in the opposite direction as the mean gas flow. Therefore, the equation of motion of a droplet can be written as

$$\frac{d\mathbf{v}_i}{dt} = (\mathbf{u}(\mathbf{x}_i, t) - \mathbf{v}_i) \frac{(1 + 0.15 \text{Re}_p^{0.687})}{\tau_p} + \left(1 - \frac{\rho_g}{\rho_l}\right) \mathbf{g}. \quad (7)$$

Here, \mathbf{v}_i is the velocity of droplet i and τ_p the droplet relaxation time given by $\tau_p = \rho_l d_i^2 / (18\mu_g)$. Moreover, $\text{Re}_p = |\mathbf{v}_i - \mathbf{u}(\mathbf{x}_i, t)| d_i / \nu$ is the droplet Reynolds number based on droplet diameter d_i and relative velocity, ρ_l is the mass density of liquid water, and μ_g the dynamic viscosity of the gas. The standard Schiller-Neumann drag correlation valid for droplet Reynolds numbers between 0 and 1000 is adopted.²⁶ Finally, \mathbf{g} denotes the acceleration of gravity. The position of droplet i , \mathbf{x}_i follows from the solution of

$$\frac{d\mathbf{x}_i(t)}{dt} = \mathbf{v}_i. \quad (8)$$

The temperature of a droplet changes by two mechanisms. The enthalpy of evaporation leads to a temperature change when a droplet evaporates or vapor condenses onto a droplet and there is convective heat transfer between the two phases. Therefore, the droplet temperature equation can be

written as

$$\rho_l c_l \mathbf{V}_i \frac{dT_i}{dt} = (h_v - h_l) \frac{dm_i}{dt} + h_m A_i (T_g(\mathbf{x}_i, t) - T_i), \quad (9)$$

where c_l is the specific heat capacity of liquid water, m_i and T_i are the mass and temperature of droplet i and h_v , and h_l are the specific enthalpy of liquid water and water vapor evaluated at the temperature of the droplet. The convective heat transfer coefficient, h_m is chosen according to the correlation for forced convection around a sphere,⁵

$$\frac{h_m d_i}{k_g} = 2 + 0.6 \text{Re}_p^{1/2} \text{Pr}^{1/3}, \quad (10)$$

where Pr is the Prandtl number of the carrier gas.

For the mass transfer, we also follow Bird *et al.*⁵ and solve

$$\frac{dm_i}{dt} = - \frac{m_i \text{Sh}}{3 \tau_p \text{Sc}} \ln \left(\frac{1 - x_{v,\delta}}{1 - x_{v,0}} \right), \quad (11)$$

where the Schmidt number $\text{Sc} = \mu_g / (\rho_g \mathcal{D})$, and $x_{v,\delta}$ and $x_{v,0}$ are the vapor mass fractions in the surroundings of the droplet and at the surface of the droplet, respectively. The latter follows from the condition of saturation, where we use Antoine's law for the saturation pressure as a function of temperature.²⁷ The Sherwood number is given by⁵ $\text{Sh} = 2 + 0.6 \text{Re}_p^{1/2} \text{Sc}^{1/3}$. All details of the model, including the values of the physical properties, can be found in Russo *et al.*²

The two-way coupling terms in the governing equations for the gas phase can be found from the requirements that they are only non-zero at the locations of a droplet and that the interaction between the two phases does not change total mass, momentum, and energy of the two-phase system. The two-way coupling term in the Navier-Stokes equation for the gas phase (2) can therefore be written as

$$\mathcal{L}_u = - \sum_{i=1}^N \frac{d(m_i \mathbf{v}_i)}{dt} \delta(\mathbf{x} - \mathbf{x}_i) = - \sum_{i=1}^N m_i \frac{d\mathbf{v}_i}{dt} \delta(\mathbf{x} - \mathbf{x}_i) - \sum_{i=1}^N \mathbf{v}_i \frac{dm_i}{dt} \delta(\mathbf{x} - \mathbf{x}_i), \quad (12)$$

where $\delta(\mathbf{x})$ is the Dirac Delta function. The two-way coupling term in water vapor equation (3) is given by

$$\mathcal{L}_v = - \sum_{i=1}^N \frac{dm_i}{dt} \delta(\mathbf{x} - \mathbf{x}_i). \quad (13)$$

Finally, the two-way coupling term in gas temperature equation (4) follows from conservation of energy and using (9),

$$\mathcal{L}_{2\text{way}} = - \sum_{i=1}^N [c_{p,v} T_i + (c_{v,a} - c_{v,v}) T_g] \frac{dm_i}{dt} \delta(\mathbf{x} - \mathbf{x}_i) - \sum_{i=1}^N h_m A_i (T_g - T_i) \delta(\mathbf{x} - \mathbf{x}_i). \quad (14)$$

This concludes the description of the physical model considered in this paper, except for the collision model which will be described in Subsection II D.

C. Numerical methods

The physical model presented in Subsections II A and II B is applied to DNS of turbulent channel flow laden with droplets. Apart from the collision model, that will be described in Subsection II D, the method is the same as used by Russo *et al.*² and based on a method for incompressible particle-laden turbulent channel flow.²⁸ The method is pseudo-spectral, consisting of a Fourier-Galerkin method in the periodic streamwise and spanwise direction and a Chebyshev-collocation method in the wall-normal direction. The time integration method of the gas phase is a combination of a third-order accurate explicit Runge-Kutta method and the implicit Crank-Nicolson method. The latter is applied to the viscous and pressure term, whereas the former treats all nonlinear terms and two-way coupling terms. These terms are calculated in physical space,

using fast Fourier transform and the 3/2-rule for de-aliasing. The velocity field is divergence free up to machine precision by the use of the influence matrix method.²⁹ At the walls, no-slip conditions are applied for the gas velocity. Moreover, a heat flux through the wall, constant in space and time, is applied for the gas temperature equation in such a way that the total energy of the system remains constant in time, and the diffusive flux of water vapor through the walls is set equal to zero.

The droplet equations are integrated in time using the forward Euler method on a partial time step in each stage of the Runge-Kutta method applied for the gas phase. This reduces the accuracy of the time integration method for the droplets to first order.¹¹ However, the time step is chosen so small that this does not significantly influence the statistical properties of the solution. A higher-order time integration method, such as the Runge-Kutta method used in previous work,^{2,28} would greatly complicate the treatment of droplet collisions.

Gas properties are interpolated to the positions of the droplets by tri-linear interpolation. The same weights as in the tri-linear interpolation are used to distribute the two-way coupling terms over the 8 neighboring grid points.^{1,2} For the droplets, just as for the gas, periodic conditions are applied in the streamwise and spanwise directions. That implies that a droplet re-enters the domain on the opposite side to where it left with the same properties.

D. Collision algorithm

The algorithm used for collisions of two droplets consists of two elements: the collision detection and the calculation of droplet properties after the collision. In this work, a simplified version of the model by Hoomans *et al.*¹³ and later modified by Vreman¹¹ is applied. The simplification is that droplet rotation is not taken into account.

In order to detect all collisions between two droplets within one stage of a Runge-Kutta time step, the computational domain is divided into a large number of rectangular blocks. These blocks are so small that they contain only a small number of droplets at most, but so large that a droplet cannot travel so far within one stage that it collides with a droplet that started in a non-neighboring block. Therefore, the search for colliding droplets can be limited to droplets within one block or two neighboring blocks, taking into account the periodic conditions in the streamwise and spanwise directions. If the number of droplets per block is not large compared to one, this changes the computational cost of the detection algorithm from order N_d^2 to order $N_d \log(N_d)$ with N_d the number of droplets.

A collision is detected if the distance between the centers of two droplets is equal to the sum of their radii during the stage of a time step. Assuming constant velocity during this partial time step, the time of collision and the positions of the two droplets at the time of collision can be determined. The components of the velocity after the collision then follow from conservation of momentum and the restitution coefficient. The droplets keep these velocities during the remainder of the partial time step, if they do not collide again before the end of the partial time step. Collisions with a wall are treated in the same way, where the walls are considered as perfectly smooth. After a collision, only the wall-normal velocity of the droplet is changed based on the restitution coefficient. For both droplet-droplet and droplet-wall collisions, we assume that part of the energy is converted into heat. This is quantified by the restitution coefficient, e . The normal component of the relative velocity before and after a collision satisfies¹³

$$\mathbf{v}_{ab} \cdot \mathbf{n} = -e \mathbf{v}_{ab,0} \cdot \mathbf{n}, \quad (15)$$

where \mathbf{v}_{ab} and $\mathbf{v}_{ab,0}$ denote the relative velocity of droplets a and b after and before a collision and \mathbf{n} is the vector pointing from the center of droplet a to the center of droplet b at the moment of collision. It is assumed that the components of the relative velocity perpendicular to \mathbf{n} are unchanged during a collision. This leads to the following relations between the velocities before and after a collision:

$$\begin{aligned} \mathbf{v}_a &= \mathbf{v}_{a,0} - \frac{(1+e)(\mathbf{v}_{ab,0} \cdot \mathbf{n})\mathbf{n}}{1+m_a/m_b}, \\ \mathbf{v}_b &= \mathbf{v}_{b,0} + \frac{(1+e)(\mathbf{v}_{ab,0} \cdot \mathbf{n})\mathbf{n}}{1+m_b/m_a}, \end{aligned} \quad (16)$$

where m_a and m_b denote the masses of droplets a and b and the subscript 0 refers to the pre-collision values. We consider two cases for the restitution coefficient. Collisions are either fully elastic, which corresponds to $e = 1$ and conservation of kinetic energy during a collision, or we use $e = 0.9$, which agrees with the literature results for small droplets.²¹

The collision model applied here is not very sophisticated. In reality, droplet rotation may play a role and droplets might coalesce instead of bounce. Moreover, if a droplet collides with a wall, it might stick to it forming a liquid film, or it might splash and break into several small droplets, depending on its impact velocity. However, since gravity is either absent or in the streamwise direction, the wall-normal velocity of a droplet is, in general, very small when it collides with a wall, which prevents it from breaking up. Moreover, the formation of a liquid film can be prevented if the wall is hydrophobic. Coalescence of two colliding droplets takes place in a certain range of Weber numbers and diameter ratios.^{18,20} It will be shown in Sec. III that the Weber number in the present simulations is so small that coalescence is very unlikely to occur.

The collision model greatly increases the computational requirements of one time step, even in the most efficient case of 1–2 droplets per block on average. The reason is not only the increase in floating point operations but also the lack of parallelizability of the present collision algorithm. While the program without the collision part has been efficiently parallelized with OpenMP, the collision algorithm runs only on a single processor in the present implementation. As a result, the CPU time for one step is larger by a factor of 4, when the program is run on 16 processors and for the highest droplet volume fraction considered in this paper. Presently, we are studying ways to parallelize the collision algorithm, but it appears that this is not possible without sacrificing the detection of all collision pairs.

III. DROPLET CONCENTRATION

In this section, the effects of droplet collisions on droplet concentration will be studied. First, a description of the test cases will be given. The flow studied is droplet-laden turbulent channel flow. The dimensions of the domain are $4\pi H$ in streamwise (x -)direction, $2H$ in wall-normal (y -)direction, and $2\pi H$ in spanwise (z -)direction, where $H = 2$ cm is half the channel height. The simulations are started from a fully developed turbulent velocity field at a frictional Reynolds number $Re_\tau = 150$ based on the friction velocity and half the channel height, which corresponds to a bulk velocity of 1.65 m/s. Initially, a uniform temperature of 20 °C and a uniform water vapor mass density, corresponding to a relative humidity of 100% are prescribed. The number of Fourier modes applied in both periodic directions equals 128 and 129 Chebyshev collocation points in the wall-normal direction. It has been shown³⁰ that for the present purpose, this resolution is sufficient at the present Reynolds number. For other purposes, such as accurate statistics of velocity derivatives, higher resolutions are required.^{31,32}

At the start of the simulation, a number of droplets are inserted at random locations, uniformly distributed over the computational domain and with their temperature and velocity equal to the temperature and velocity of the gas at the location of each droplet. The initial droplet diameter equals $d_i = 3.09 \times 10^{-3}H = 61.8 \mu\text{m}$, which corresponds to a Stokes number, defined as the droplet relaxation time in wall units, of 10. The heat flux applied to the walls equals 32 W/m^2 and taken in such a way that the upper wall is heated, whereas the lower wall is cooled. The driving force in the Navier-Stokes equation is defined in such a way that the total mass flow rate of gas and droplets remains approximately constant in time. All these parameters correspond to the reference test case in Russo *et al.*² The geometry of the problem studied in this paper is sketched in Fig. 1.

Various simulations have been performed for different numbers of droplets, both with and without four-way coupling. Simulations H2 and H4 (high concentration) have 2 000 000 droplets, simulations M2 and M4 (medium concentration) have half this number of droplets, and simulations L2 and L4 (low concentration) have only 500 000 droplets. The overall volume fraction, the volume of all droplets divided by the volume of the flow domain, ϕ_{overall} , is approximately 2.2×10^{-4} in cases H2 and H4. Initially, the distribution of droplets is uniform. The variations of the overall volume fraction in time are on the order of 0.1%. Two simulations without four-way coupling, H2

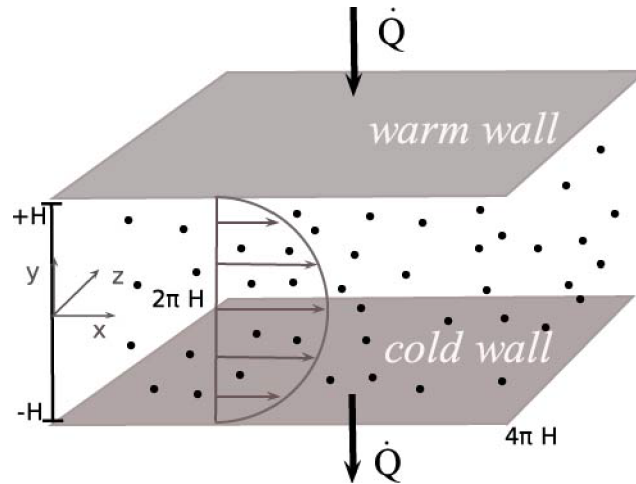


FIG. 1. Sketch of geometry. Note that in the real geometry, the coordinate system is right handed.

and M2, have also been considered by Russo *et al.* Here, specifically the effects of droplet collisions will be investigated. In these six simulations, only fully elastic collisions between droplets and the walls have been considered and gravity is not taken into account. However, in one additional simulation, M4I, a normal restitution coefficient of 0.9 has been applied for both types of collisions in order to investigate whether the elasticity of the collisions has an appreciable effect on the results. Moreover, this same case has also been carried out for upward flow, M4IG, in which gravity is pointing in the direction opposite to the mean flow. All test cases are summarized in Table I.

The heat flux applied to the upper wall leads to an increase of the gas temperature there and by convective heat transfer between gas and droplets also of the droplet temperature. The increased gas temperature results in an increase of the saturation pressure, so that locally the relative humidity will become less than 100%. Therefore, droplets near the upper wall will start to evaporate. The associated enthalpy of evaporation results in a decrease of the droplet temperature according to Eq. (9), compared to the situation with solid particles instead of droplets. Therefore, the temperature difference between gas and droplets increases compared to solid particles.² Near the lower wall, the opposite happens: the heat flux directed out of the computational domain leads to a decrease of the gas temperature and droplets and to over-saturation and hence condensation of water vapor onto the droplets. Therefore, the absolute temperature difference between gas and droplets increases compared to the case with solid particles. The effects of this on the heat transfer properties of the channel will be discussed in more detail in Sec. IV.

On a slower time scale, the droplet concentration profile across the channel will change by turbophoresis.^{33,34} The inhomogeneity of the wall-normal velocity fluctuations in turbulent channel

TABLE I. Definition of the test cases; $\phi_{overall}$ is the overall droplet volume fraction.

Case	Number of droplets	Coupling	$\phi_{overall}$	Restitution coefficient	Gravity
H2	2×10^6	Two-way	2.2×10^{-4}	...	No
M2	1×10^6	Two-way	1.1×10^{-4}	...	No
L2	0.5×10^6	Two-way	0.55×10^{-4}	...	No
H4	2×10^6	Four-way	2.2×10^{-4}	1.0	No
M4	1×10^6	Four-way	1.1×10^{-4}	1.0	No
L4	0.5×10^6	Four-way	0.55×10^{-4}	1.0	No
M4I	1×10^6	Four-way	1.1×10^{-4}	0.9	No
M4IG	1×10^6	Four-way	1.1×10^{-4}	0.9	Yes

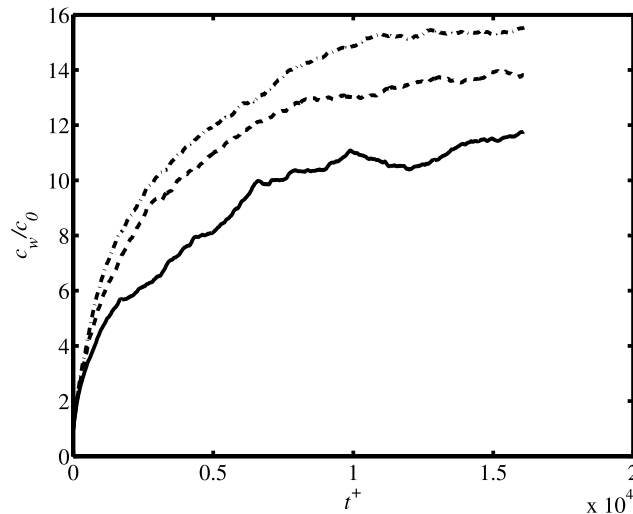


FIG. 2. Droplet concentration close to the walls as a function of time in wall units, normalized by the initial concentration; solid: H2; dashed: M2; dashed-dotted: L2. The concentration close to the wall increases because of turbophoresis.

flow leads to a gradual accumulation of droplets in the near-wall regions. This is illustrated in Fig. 2, where the droplet concentration close to the walls is shown as a function of time. To this end, the channel has been divided into 40 uniform slabs in the wall-normal direction and the number of droplets in each slab has been counted. The concentration is normalized by the initial uniform concentration (c_0) in order to better compare the three cases with different overall droplet volume fractions. Time has been expressed in wall units.

The figure shows that indeed the droplet concentration close to the walls increases in time. The reference case in Russo *et al.*² $t^+ = 2 \times 10^4$ (which corresponds to 26 s), a statistically steady state is reached, in which the droplet concentration only fluctuates in time. The maximum possible normalized wall concentration is equal to 20, if all droplets are located in the bins closest to each wall. The maximum concentration reached in case H2 is $14c_0$ and is significantly lower than in case one-way coupling is applied. The presence of the droplets attenuates the wall-normal gas velocity fluctuations, and hence the turbophoretic force. This can also be appreciated from Fig. 2, where the turbophoresis is seen to be stronger in case the overall droplet concentration is lower. The figure shows that for case H2, the droplet volume fraction close to the walls is approximately 2.5×10^{-3} , which is in the regime where droplet collisions cannot be disregarded according to the classification by Elghobashi.³

Locally, however, the droplet concentration can be an order of magnitude higher than the average concentration in a given slab. In order to see this, the total computational domain is divided into blocks and the number of droplets in each block is counted. Results depend on the number of blocks; if there are only few droplets in each block, the concentration fluctuates strongly in time. For a uniform division of the domain into 80 blocks in each direction, the volume fraction of droplets close to the lower wall is shown in Fig. 3 for the three cases employing two-way coupling. The figure shows an instantaneous result in a plane parallel to the wall at a time where the concentration has reached a statistically steady state at $t^+ = 3.8 \times 10^4$. Note that the results on both walls are qualitatively the same. Although due to phase change the droplet size near both walls is different, this has only a minor effect on the droplet concentration. This figure shows that indeed the volume fraction exhibits large variations in space. Droplets are preferentially located in the low-speed streaks close to the walls, resulting in local droplet volume fractions that are larger by a factor of ten compared to the mean volume fraction close to the wall for case H2. Also for cases M2 and L2, local droplet volume fractions much higher than the limiting value for the two-way coupling regime according to Elghobashi³ are encountered. It is evident that at least for the droplets in the locally dense regions, the omission of collisions cannot be justified. It is remarkable that cases M2 and L2 show an almost

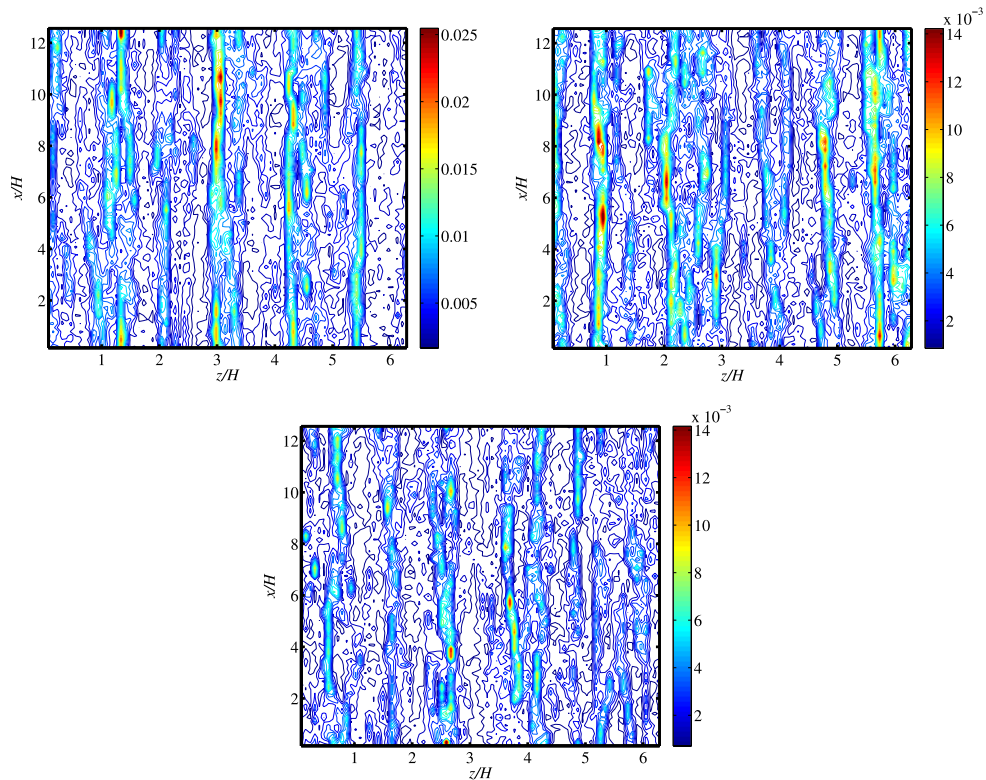


FIG. 3. Droplet volume fraction in a plane close to the lower wall; left: H2; right: M2; below: L2. The streamwise direction is denoted by x , the spanwise by z . Droplets are clustering in low-speed streaks, which are parallel to the streamwise direction.

equal maximum volume fraction, but the average value in this plane close to the wall is smaller in case L2 than in M2.

Next, the cases employing four-way coupling are considered. Figure 4 shows the droplet concentration close to the walls as a function of time for the three different overall volume fractions, along with case H2 for reference. There are two striking differences between the cases with and without four-way coupling. First, the maximum droplet concentration close to the wall is much lower when droplet collisions are taken into account. Second, the statistically steady state for droplet concentration is reached much more quickly. After $t^+ \approx 2000$, the droplet concentration only fluctuates around a mean value. This state is reached around $t^+ = 2 \times 10^4$ in the two-way coupling cases. For all three values of the overall volume fraction, four-way coupling has a large effect on droplet concentration, which shows that Elghobashi's classification can certainly not be applied to the overall volume fraction in the flow, even not if the Stokes number in wall units is fairly low.

Figure 5 shows the distribution of volume fraction in a plane close to the lower wall for the three cases with four-way coupling at $t^+ = 1.6 \times 10^4$, long after the statistically steady state for the droplet concentration has been reached. The maximum droplet concentration attained in these cases is lower by a factor of approximately 8 than in the corresponding two-way coupling cases. However, the droplets are still preferentially located in the low-speed streaks close to the walls. Figure 6 shows the droplet concentration in a plane perpendicular to the streamwise direction for the two cases with the highest overall volume fraction. In order to better visualize the results, isolines of the square root of the droplet volume fraction have been shown. The figure shows that in both cases, there are regions void of droplets, but in the two-way coupling case, these are larger. Also, in case H4, the regions with large concentrations in the low-speed streaks have a larger size in the wall-normal direction.

Next, we turn to the two cases where an additional physical effect has been considered: inelasticity of the collisions and gravity. Figure 7 shows the concentration of droplets close to the wall

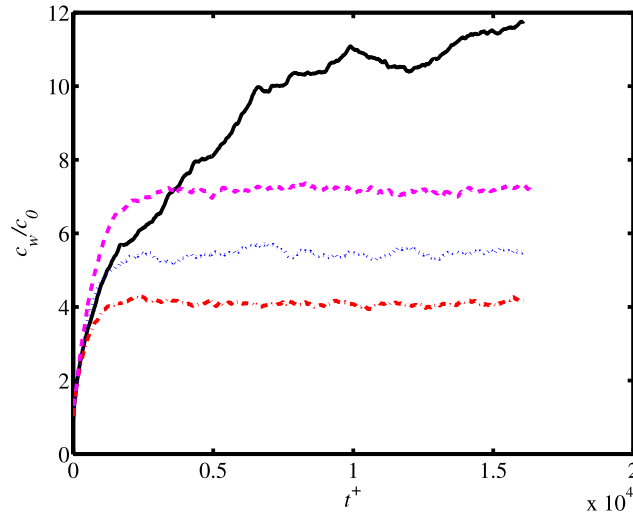


FIG. 4. Droplet concentration close to the walls as a function of time in wall units, normalized by the initial concentration; black solid: H2; red dashed-dotted: H4; blue dotted: M4; magenta dashed: L4.

as a function of time for the four cases with overall volume fraction equal to 1.1×10^{-4} . The figure shows that the restitution coefficient used in droplet-droplet and droplet-wall collisions has no appreciable effect on the mean concentration close to the wall. Also the additional effect of gravity is very small. The distribution of the volume fraction on a plane parallel and close to a wall is very similar for all three cases employing four-way coupling. Apparently, both gravity and inelasticity of the collisions do not play a significant role on the droplet distribution in this flow.

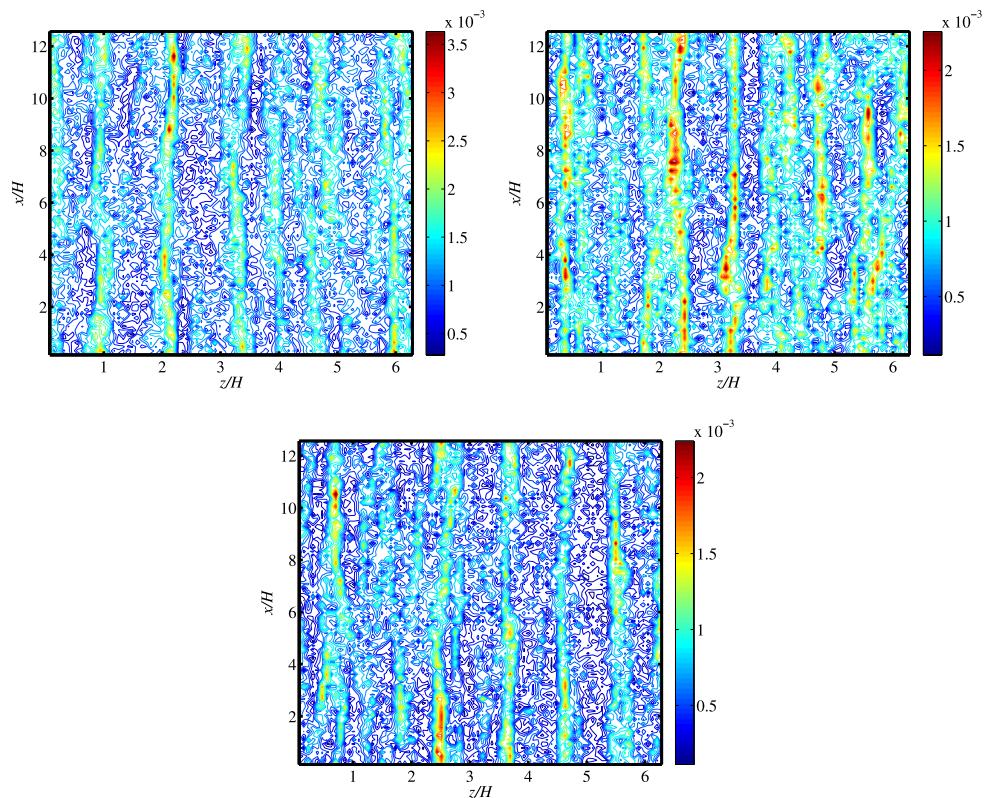


FIG. 5. Droplet volume fraction in a plane close to the lower wall; left: H4; right: M4; below: L4.

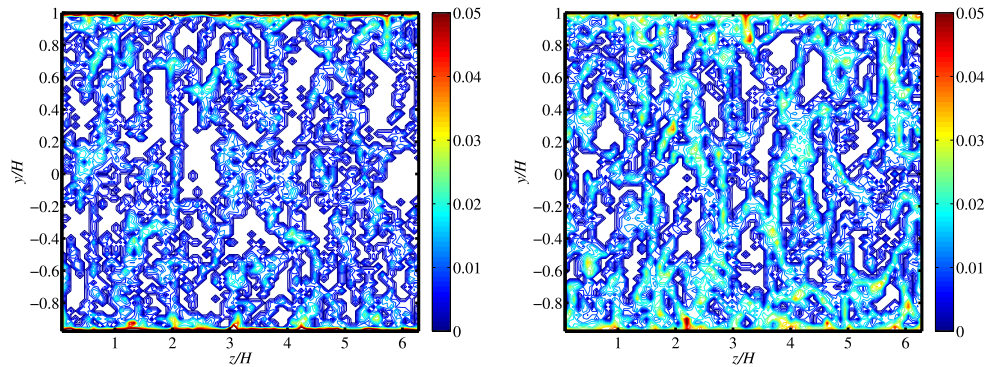


FIG. 6. Droplet volume fraction in a plane perpendicular to the streamwise direction; left: H2; right: H4. Note that isolines of the square root of droplet volume fraction are plotted.

In order to illustrate the differences between the cases with two-way and with four-way coupling with respect to the droplet volume fraction close to the walls, we calculated the mean, root-mean-square (RMS), and skewness of the droplet volume fraction in the region close to both walls by dividing the computational domain in 80 equally sized blocks in all directions. The results are collected in Table II for all test cases, where averaging over time in the statistically steady state has been applied. The most striking differences between two-way and four-way coupling are seen in the RMS and skewness. For the two-way coupling cases, the RMS is not much smaller than the mean value, whereas for the four-way coupling cases, the RMS is smaller by approximately a factor of 2 than the mean. The skewness of the droplet volume fraction close to the wall equals approximately 2 for the two-way coupling cases and is close to 1 for all four-way coupling cases. This shows that the probability distribution function of the two-way coupling cases is much more skewed toward large values in case of two-way coupling. When collisions are included, high local values of droplet concentration are less likely to occur. Non-sticking collisions lead to more random motion of the particles, and thereby smoothen maxima of the local droplet concentration. As a further illustration of this, we show the probability density functions for cases M2 and M4 in Fig. 8. It is clear from the figure that not only the mean value is much larger in case of two-way coupling, but the probability distribution function also extends to much higher volume fractions.

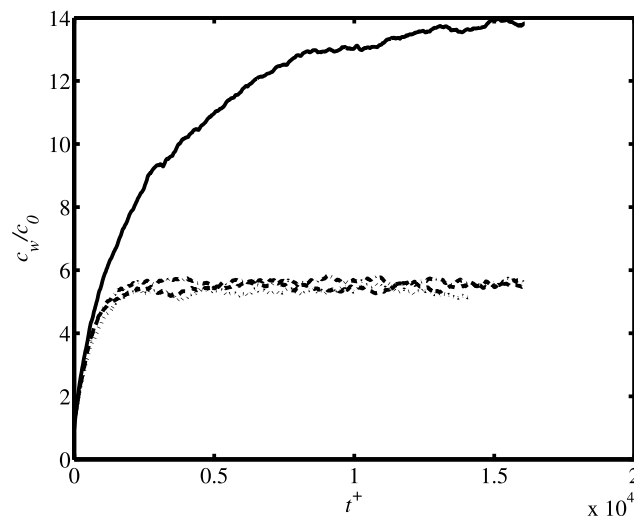


FIG. 7. Droplet concentration close to the walls as a function of time in wall units, normalized by the initial concentration; solid: M2; dashed: M4; dashed-dotted: M4I; dotted: M4IG.

TABLE II. Mean, RMS, and skewness of droplet volume fraction close to the wall for all test cases, calculated by dividing the computational domain in 80 blocks in each direction.

Case	$\langle \phi_w \rangle$	$\text{RMS}(\phi_w)$	$S(\phi_w)$
H2	4.5×10^{-3}	3.0×10^{-3}	1.96
M2	2.7×10^{-3}	2.1×10^{-3}	1.93
L2	1.47×10^{-3}	1.21×10^{-3}	2.11
H4	1.07×10^{-3}	4.3×10^{-4}	0.81
M4	7.9×10^{-4}	3.7×10^{-4}	0.91
L4	5.6×10^{-4}	3.0×10^{-4}	1.04
M4I	8.2×10^{-4}	3.9×10^{-4}	0.94
M4IG	8.0×10^{-4}	4.0×10^{-4}	1.04

To obtain a meaningful local average, the size of the blocks in which we divide the computational domain should evidently be larger than the droplet size, but smaller than the large scales of the turbulence. Since there is no clear physical scale separation between the droplet size and the large scales of the turbulence, the local volume fraction field, obtained with a volume average acting in this range of scales, will to some extent depend on the volume of the local volume averaging operator. In this respect, the local volume averaging operator is similar to the spatial filter in large-eddy simulation, where the RMS of a filtered variable also depends on the filter size. Thus, the magnitudes of RMS, skewness, and probability density function of the local volume fraction field extracted from our DNS depend on the number of blocks used. If we use, for example, 40 blocks instead of 80 blocks in each homogeneous direction, keeping the number of blocks in the wall-normal direction equal to 80, the skewness in case M2 drops from 1.93 to 1.34, while the skewness in case M4 drops from 0.91 to 0.65. The effect of collisions on the skewness appears to be less sensitive to the number of blocks: the numbers mentioned show that collisions reduce the skewness by about a factor of two, both for 40 and 80 blocks.

IV. COLLISION FREQUENCY

In this section, we will consider the collision frequency found in the simulations and compare it with results from the literature. To that end, we divided the wall-normal direction in 80 equally

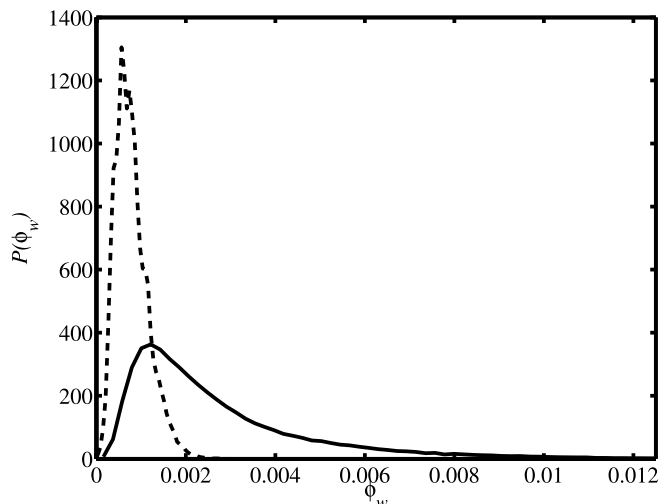


FIG. 8. Probability density function of droplet volume fraction close to the walls, calculated by dividing the computational domain in 80 blocks in each direction; solid: M2; dashed: M4.

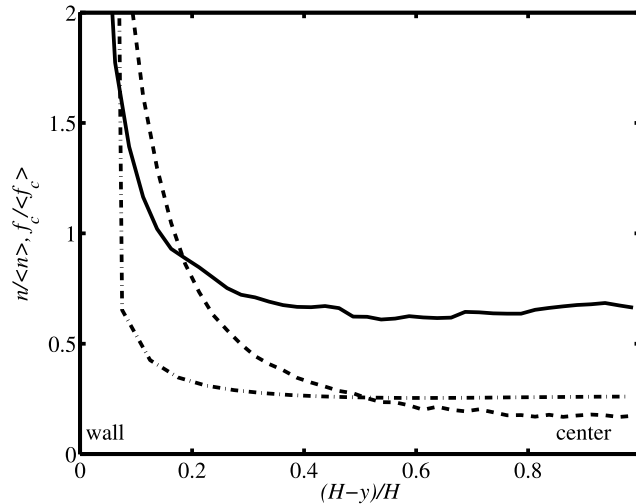


FIG. 9. Droplet number density (solid) and collision frequency (dashed) as functions of the distance to the wall for case M4 and droplet number density for case M2 (dashed-dotted). All quantities are normalized with their mean value.

sized slabs and counted the number of droplets and the number of collisions within each slab during a sufficiently long time interval of the simulation. Figure 9 shows for case M4, the droplet number density and the collision frequency as functions of the wall-normal coordinate, along with the droplet number density of case M2. Results have been averaged over both halves of the channel, as the difference between them is not significant. All quantities in the figure are normalized by their mean value. The difference in droplet number density between cases M2 and M4 again shows the large effect of including droplet collisions on the droplet concentration profile. Moreover, as a result of the non-uniform droplet concentration in case M4, the collision frequency, defined as the number of collisions per unit time per unit volume is even more non-uniform. The results in this figure can be compared to the results by Yamamoto *et al.*¹⁰ for lycopodium particles (Figure 10d in the reference). In view of the differences between the two simulations, in particular, also the fact the Yamamoto *et al.* employed large-eddy simulation for the gas phase, the qualitative agreement between the results is good.

Sundaram and Collins⁶ studied the collision statistics in DNS of homogeneous, isotropic turbulence for particles with various Stokes numbers and compared the results with a theoretical expression. They argued that the collision frequency, f_c , depends on the particle number density, n , the particle diameter, d , the relative velocity v_r , and the particle radial distribution function, $g(r)$, according to

$$f_c = \frac{1}{2} \pi d^2 n^2 g(d) v_r, \quad (17)$$

where v_r is the mean relative velocity of two colliding particles and $g(d)$ is the particle radial distribution function at contact, when the distance between two particles is equal to the particle diameter. In our present simulations, the droplet diameter is not constant, but the changes are so small that we will assume in the subsequent analysis that the droplet diameter remains equal to its initial value. In contrast to the case of homogeneous, isotropic turbulence studied by Sundaram and Collins, the droplet number density, the mean relative velocity, and the droplet radial distribution function may depend on the wall-normal coordinate in our study of turbulent channel flow. Therefore, we evaluate the quantities appearing in (17) as a function of the wall-normal coordinate by dividing the wall-normal direction in 80 equally sized slabs. In that way, the collision frequency, the droplet number density, and the relative velocity can be determined as functions of the wall-normal coordinate. From (17), the unknown quantity $g(d)$ can then be determined as it is the only unknown.

By varying the particle diameter, Sundaram and Collins performed simulations for various Stokes numbers, where the Stokes number in their case is the ratio of the particle relaxation time

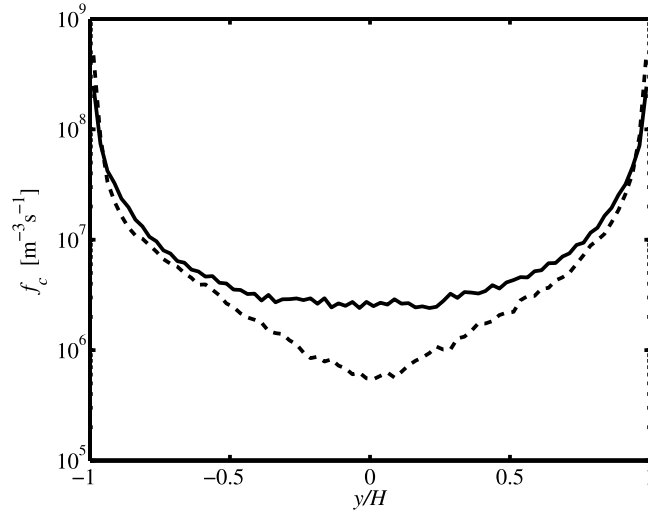


FIG. 10. Droplet collision frequency (solid) in number of collisions per unit volume and per unit time and $\frac{1}{2}\pi d^2 n^2 v_r$ (dashed) as functions of the wall-normal coordinate for case M4.

and the Kolmogorov time. They found that $g(d)$ is a function of the Stokes number. We only considered droplets of one diameter, but in our case, the Kolmogorov time depends on the wall-normal coordinate. Therefore, we can consider particles with Stokes numbers ranging from 1 (at the center of the channel) to 4 (at the wall). Figure 10 shows for case M4, the collision frequency as a function of the wall-normal coordinate, along with the right-hand side of (17) for $g(d) = 1$. The results show that the radial distribution function at contact, $g(d)$, varies with the wall-normal coordinate. The results show that the collision frequency is particularly high close to the walls of the channel, where the local droplet concentration is the highest. The non-uniformity of the droplet concentration, caused by turbophoresis, is the main reason for the large effect of droplet collisions on the concentration results shown in Sec. III.

By dividing the two lines shown in Fig. 10, $g(d)$ can be determined as a function of the Stokes number. The result is shown in Fig. 11 for cases H4, M4, and L4 and compared with the results by Collins and Sundaram. There are two reasons why the results for $g(d)$ are not so smooth. First, close to the wall, the Kolmogorov time has a local minimum, which leads to the sudden

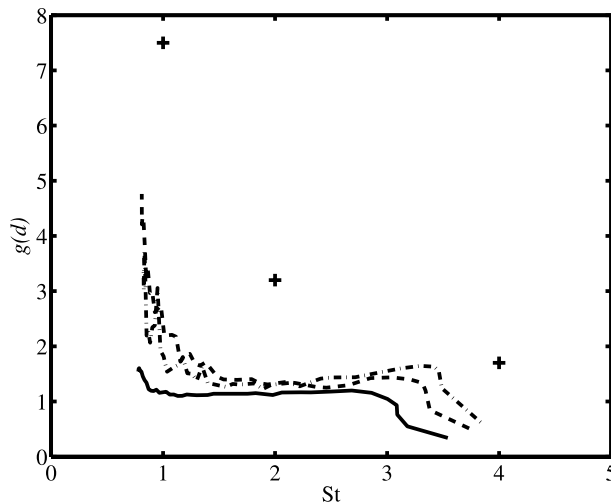


FIG. 11. Radial distribution function at contact determined from (17); solid: H4, dashed: M4, dashed-dotted: L4. The symbols are taken from Sundaram and Collins.⁶

jump in $g(d)$ near $St = 3.5$. Second, in the center of the channel, the droplet number density and, in particular, the collision frequency are so small that the determination of $g(d)$ is less accurate. Both our present results for cases M4 and L4 and the results by Sundaram and Collins show that the particle radial distribution function at contact decreases for increasing Stokes number. Note, however, that Sundaram and Collins found a sharp maximum in $g(d)$ at $St = 0.5$. Apart from that, there is a substantial difference in the value of $g(d)$ of approximately a factor of 2, which may be attributed to the differences between the two flows considered. Since the radial particle distribution function is highly dependent on preferential concentration, differences between homogeneous and inhomogeneous flows can be expected. At the channel center, where St is small, $g(d)$ is much larger than 1 for cases M4 and L4. For case H4, such high values of $g(d)$ in the center of the channel are not observed. This may be attributed to the higher mean droplet volume fraction in the center of the channel for this case and the resulting increased effect of collisions there.

One of the quantities contributing to the collisions frequency is the mean relative velocity of two colliding droplets. In Fig. 12, this quantity is shown as a function of the wall-normal coordinate and compared with the mean relative velocity of all particle pairs within a slab in the wall-normal direction. The figure shows that the shape of these two mean relative velocities is similar, but the mean relative velocity of two colliding droplets is significantly smaller than the mean relative velocity of all droplet pairs. The same observation was made by Sundaram and Collins⁶ for homogeneous, isotropic turbulence. The reason is that droplets that collide must be close and have a larger chance that their velocities are correlated than droplets that are further apart, because of the interaction between droplets and gas. It can be expected that very large droplets, which respond to the gas flow much more slowly, behave more randomly. This will lead to a higher relative velocity of two colliding droplets.

As a last topic of this section, we investigate other properties of droplet pairs that collide. During the statistically steady state of the cases with four-way coupling, the Weber number of all colliding droplet pairs was monitored during a certain time interval. The Weber number is defined here as

$$We = \frac{\rho_l v_{rel}^2 d_i}{\sigma}, \quad (18)$$

where σ is the surface tension of water in air, v_{rel} is the magnitude of the relative velocity of the two colliding droplets, and d_i is the diameter of the smallest of the two droplets. The maximum Weber number found was approximately 1.5 and less than 0.04% of all collisions occurred at $We > 1$. The mean value of the Weber number of all colliding droplets was 0.057 for case H4 and

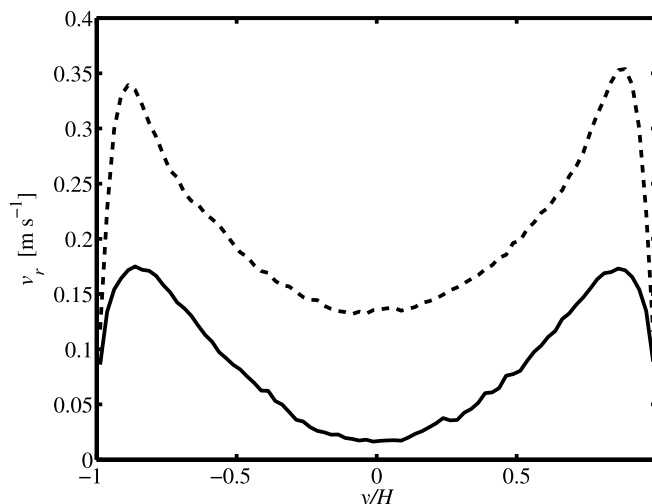


FIG. 12. Mean relative velocity of two colliding droplets (solid) and of all droplet pairs (dashed) as functions of the wall-normal coordinate for case M4.

0.043 for case M4. This makes clear that the assumption that colliding droplets do not coalesce but bounce is justified according to experimental results for colliding droplets.^{18–20} Ko and Ryou³⁵ used a combination of two conditions for grazing bounce collisions between two droplets, based on the work of O'Rourke.³⁶ Colliding droplets bounce if the Weber number is sufficiently small and if the angle between their relative velocity and separation vector is larger than a critical value that depends on the Weber number and the diameter ratio. It appears that the combination of these two conditions is satisfied in 95% of all collisions in the simulations reported here. For collisions between a droplet and the wall, the mean value of the Weber number is even an order of magnitude smaller, while the maximum value found was 0.36. Since the diameter of all droplets does hardly change during the simulation, the reason for the low value of the Weber number is the low relative velocity. As already observed above, due to the rather low value of the droplet relaxation time, the droplets quickly adjust to the local velocity. Therefore, neighboring droplets do not have a large difference in velocity.

V. THERMAL PROPERTIES

In the paper on heat transfer enhancement in turbulent channel flow by inertial solid particles,¹ it has been shown that the heat transfer across the channel can be quantified by the Nusselt number, defined as

$$\text{Nu} = \frac{2H}{\Delta T_g} \left. \frac{d\langle T_g \rangle}{dy} \right|_{\text{wall}}, \quad (19)$$

where brackets denote averages over the homogeneous directions and time, the wall-normal derivative is evaluated at a wall, and ΔT_g is the temperature difference between the two walls. Moreover, the Nusselt number can be split into three parts according to $\text{Nu} = \text{Nu}_{\text{lam}} + \text{Nu}_{\text{turb}} + \text{Nu}_{\text{part}}$. This follows from averaging the gas temperature equation over time and the homogeneous directions and integration of the result twice over the wall-normal direction.^{1,2} The first contribution, $\text{Nu}_{\text{lam}} = 1$, is the Nusselt number for laminar flow without particles. The second contribution is due to turbulence,

$$\text{Nu}_{\text{turb}} = -\frac{1}{\alpha \Delta T_g} \int_{-H}^H \langle u'_y T'_g \rangle dy, \quad (20)$$

where a prime denotes the fluctuating part of a quantity, $\alpha = k_g / (\rho_g c_g)$ is the thermal diffusivity of the gas, and u_y is the wall-normal velocity component of the gas. Finally, the third contribution Nu_{part} is due to the particles by the two-way coupling term in the equation for the gas temperature, but note that the presence of particles also influences the second contribution. The third contribution can be approximated by

$$\text{Nu}_{\text{part}} \approx -\int_{-H}^H \int_{-H}^y \frac{2\pi n(s) d_p \langle T_g - T_p \rangle}{\Delta T_g} ds dy, \quad (21)$$

where $n(s)$ is the local particle number density, which depends on the wall-normal coordinate, d_p and T_p denote particle diameter and particle temperature, and the gas temperature is evaluated at the particle position. The large increase in Nusselt number when inertial particles are present could be fully attributed to Nu_{part} , since Nu_{turb} even decreased in the presence of particles, and was explained by the combination of the high particle concentration close to the walls and the temperature difference between particles and gas there.¹

Russo *et al.*² showed that in the present case of evaporating droplets instead of solid particles, there are some extra contributions to the expression for the Nusselt number (19), but they were shown to be negligibly small in all cases considered. Compared to solid particles, droplets lead to a larger increase in Nusselt number, since the enthalpy of evaporation related to phase change results in a higher temperature difference between droplets and gas.

Both studies^{1,2} did not take particle or droplet collisions into account. In Sec. III, it has been shown that droplet collisions result in significantly lower droplet concentrations close to the wall. Therefore, the argument of high concentration in the regions where the temperature difference

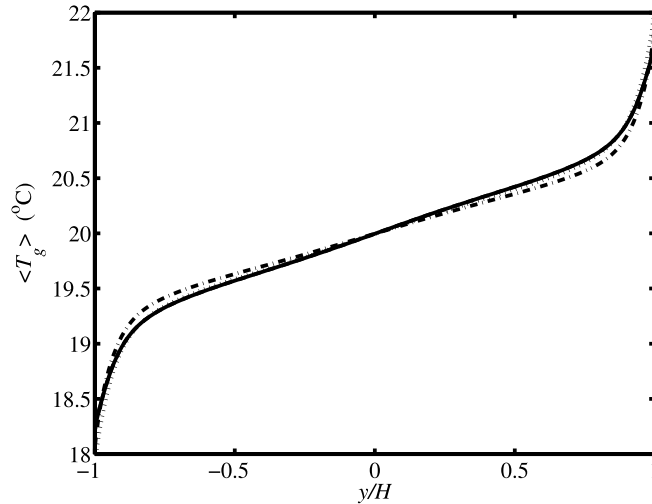


FIG. 13. Mean temperature as a function of the wall-normal coordinate in the statistically steady state; solid black: H2; dashed black: M2; dashed-dotted red: H4; dotted blue: M4. The mean temperature is averaged over the streamwise and spanwise directions and over time in the steady state.

between the continuous and dispersed phase is the largest (used in these papers to explain the large value of Nu_{part} according to (21)) cannot be applied to the present cases with four-way coupling. In this section, the effect of four-way coupling on the mean temperature profile in the channel will be investigated, and its effect on the heat transfer across the channel will be quantified by the Nusselt number.

Figure 13 shows the mean temperature profile across the channel for four of the cases studied in this work. The results are averaged over the two homogeneous directions and over time in the statistically steady state. The results of the four cases shown here are quite close, but some differences can be seen, especially in the temperature close to the walls. For the present settings, where the heat flux at the walls is fixed, the magnitude of the temperature difference between the walls is a direct measure for the Nusselt number according to Eq. (19). The Nusselt numbers in the steady state are listed in Table III. As already found by Russo,² a lower overall droplet volume fraction results in a somewhat smaller Nusselt number and this tendency is retained for the lowest overall droplet volume fraction studied here. Also, four-way coupling yields a reduced Nusselt number as compared to the same case with only two-way coupling, but the reduction in Nusselt number is much less than the reduction in droplet concentration close to the walls. For all overall volume fractions considered here, the Nusselt number is reduced by only approximately 17% if four-way coupling is employed. Note that the Nusselt number for the same non-isothermal flow without droplets or particles² equals 4.4, which shows that the increase of the Nusselt number by the presence of droplets remains significant if droplet collisions are taken into account. It is remarked

TABLE III. Nusselt number and its contributions for all test cases.

Case	Nu	Nu_{lam}	Nu_{turb}	Nu_{part}
H2	15.6	1.0	3.1	11.5
M2	14.1	1.0	3.1	10.0
L2	12.4	1.0	3.2	8.2
H4	13.0	1.0	2.3	9.7
M4	11.9	1.0	2.5	8.4
L4	10.8	1.0	2.6	7.2
M4I	11.9	1.0	2.5	8.4
M4IG	12.6	1.0	2.7	8.9

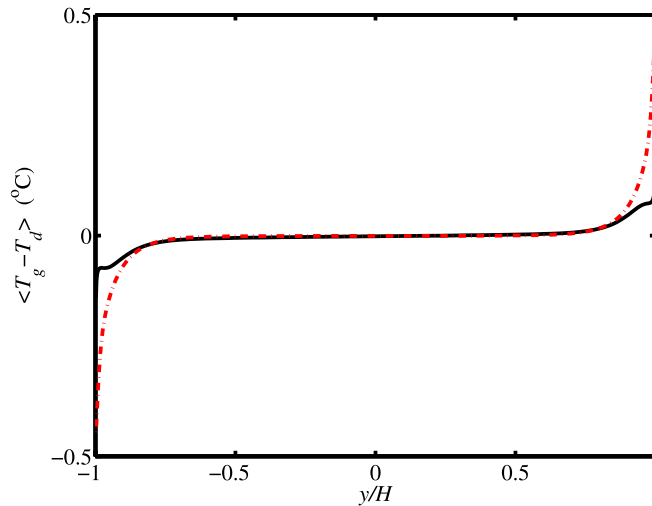


FIG. 14. Mean temperature difference between gas and droplets as a function of the wall-normal coordinate in the statistically steady state; solid black: H2; dashed-dotted red: H4. The mean temperatures are averaged over the streamwise and spanwise directions and over time in the steady state.

that inelasticity of collisions does not have any effect on the Nusselt number for the restitution coefficient of 0.9 adopted here. Finally, the test case in which gravity is included shows a slightly increased Nusselt number compared to the same case without gravity.

Since collisions reduce the droplet concentration close to the walls by almost a factor of three (see Fig. 4), one of the other contributions to the expression for Nu_{part} given by (21) must be simultaneously increased by almost the same factor. The droplet diameter in (21) is not the reason for this. The mean droplet diameters as a function of the wall-normal coordinate resulting from cases H2 and H4 are almost indistinguishable. The absolute temperature difference between gas and droplets, however, is significantly increased by the droplet collisions, as illustrated in Fig. 14, which shows the mean temperature difference between gas and droplets as a function of the wall-normal coordinate in the statistically steady state. Close to the upper (warm) wall, the mean droplet temperature is almost unchanged by the effects of collisions. This temperature is mainly determined by the rate of evaporation, which is almost equal in the two cases, as evidenced by the unchanged mean

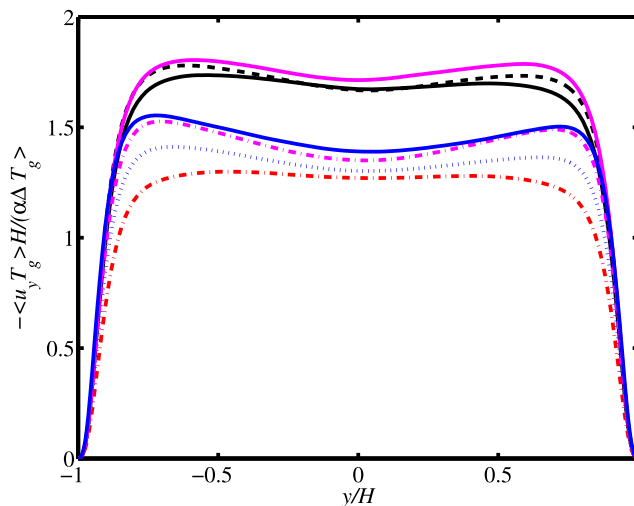


FIG. 15. Non-dimensionalized contribution $-\langle u_y T_g' \rangle H / (\alpha \Delta T_g)$ to the Nusselt number according to Eq. (20) as a function of the wall-normal coordinate; solid black: H2; dashed black: M2; solid magenta: L2; dashed-dotted red: H4; dotted blue: M4; dashed magenta: L4; solid blue: M4IG. The integral of the plotted quantity over y is equal to the contribution Nu_{urb} to the Nusselt number.

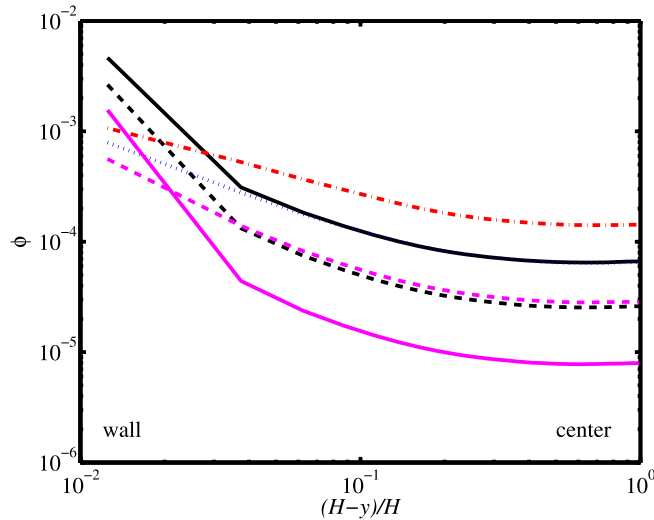


FIG. 16. Mean droplet volume fraction as a function of the wall-normal coordinate, $(H-y)/H$, averaged over time in the steady state and over the two halves of the channel; solid black: H2; dashed black: M2; solid magenta: L2; dashed-dotted red: H4; dotted blue: M4; dashed magenta: L4.

droplet diameter. The mean gas temperature, however, is significantly higher if droplet collisions are taken into account. The reason is that the convective heat transfer between droplets and gas transfers less energy from the droplets to the gas, since the surface area of droplets present in this region is much less. Close to the lower (cold) wall, the argument is opposite.

The reduction of the Nusselt number due to four-way coupling is not only caused by the difference in Nu_{part} but also by a reduction in the turbulent contribution Nu_{turb} , as can be seen in Fig. 15, where the term $-\langle u'_y T'_g \rangle H / (\alpha \Delta T_g)$, which appears in the integral in Eq. (20), is shown as a function of the wall-normal coordinate for most of the cases considered here. Case M4I is not included since it coincides with case M4. The contribution Nu_{turb} is the integral of the quantity shown in the figure. The figure shows that the central region of the channel is most important for this contribution. Droplet collisions lead to higher droplet concentrations in the central region of the channel, especially in case H4, where the droplet volume fraction is the highest. All three non-negligible contributions to the Nusselt number are shown in Table III. The attenuation of the

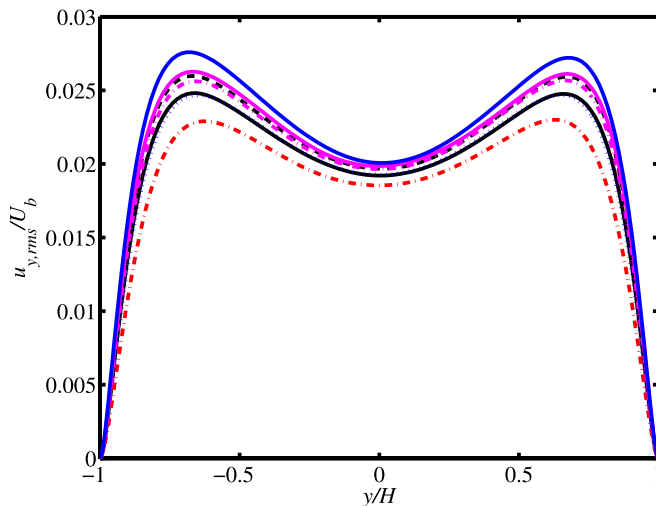


FIG. 17. RMS of wall-normal fluid velocity fluctuations scaled with the bulk velocity as a function of the wall-normal coordinate; solid black: H2; dashed black: M2; solid magenta: L2; dashed-dotted red: H4; dotted blue: M4; dashed magenta: L4; solid blue: M4IG.

correlation of the wall-normal gas velocity and the temperature by the collisions can be understood from the higher droplet concentration in the central region of the channel.

The time-averaged droplet volume fraction profiles for almost all cases are shown in Fig. 16, where logarithmic scaling and averaging over the two halves of the channel have been used for better clarity. The results of simulations M4I and M4IG are almost indistinguishable from the results of M4 and are not shown here. The higher droplet concentration in the center of the channel for the cases with four-way coupling also results in reduced fluid velocity fluctuations in the wall-normal direction there, as is shown in Fig. 17. A similar decrease can be found in the spanwise velocity fluctuations, whereas the streamwise velocity fluctuations are almost not affected by the droplet collisions and the resulting changed droplet concentration. A remarkable result is the higher level of the wall-normal velocity fluctuations found in the case with gravity.

VI. CONCLUSIONS

In this paper, the effect of droplet collisions on droplet concentration and on the gas temperature profile has been investigated in droplet-laden differentially heated turbulent channel flow by means of DNS and employing a Lagrangian point-particle approach for the droplets. All collisions between two droplets have been taken into account by a deterministic approach. Results with and without four-way coupling have been compared for three different overall droplet volume fractions and the effects of inelastic collisions and gravity in the upstream direction have been considered.

It has been found that local droplet volume fractions close to the channel walls become so high due to turbophoresis and preferential concentration, that collisions have a large effect on droplet concentration, even though the domain-averaged droplet concentration is within the regime for two-way coupling according to the classification by Elghobashi.³ For dilute gas-solid flow, it is known that collisions can strongly reduce the particle concentration near the wall, at least when the Stokes number is sufficiently high.⁹⁻¹¹ Elghobashi's diagram³ indicates that the demarcation line between the two-way and four-way coupling regimes shifts toward lower volume fraction if the Stokes number becomes higher. However, in the present work, the Stokes number is only 10 in wall units, which shows that the effect of collisions on concentration in dilute flows is not limited to very high Stokes numbers. Moreover, a steady concentration profile is reached in a much shorter time than when only two-way coupling is applied. In addition, the positive skewness of the local droplet volume fraction distribution near the walls is reduced by a factor of two. From the calculated collision frequency, the droplet radial distribution function at contact has been determined and found to depend on the Stokes number based on the Kolmogorov time in a qualitatively similar way as found by Sundaram and Collins⁶ for homogeneous, isotropic turbulence, although the value is about a factor of two lower.

In spite of the much lower droplet concentration close to the walls, the increase in heat transfer, quantified by the Nusselt number, compared to the same flow without droplets, is only moderately decreased by the effect of droplet collisions. That the decrease is only moderate has been explained by the higher temperature difference between droplets and gas close to the walls, which is due to the lower heat-exchange area available. The higher droplet concentration in the central part of the channel compared to two-way coupling only results in a decrease in the wall-normal and spanwise gas velocity fluctuations.

In the present work, it has been assumed that droplets always bounce during a collision. The low value of the Weber number and relatively high grazing angle of two colliding droplets for most of the collisions show that this assumption is justified.

ACKNOWLEDGMENTS

This work was sponsored by the Stichting Nationale Computerfaciliteiten (National Computing Facilities Foundation, NCF) for the use of supercomputer facilities, with Financial support from the Nederlandse Organisatie voor Wetenschappelijk Onderzoek, NWO. The first author developed a collision algorithm based on the source code of the collision module written by Vreman,¹¹ while the latter was with official permission produced using knowledge of the source code of the collision

module written by Kuipers, Hoomans, Link, Bokkers, and Deen, Chemical Reaction Engineering Group, University of Twente (see Hoomans *et al.*¹³).

- ¹ J. G. M. Kuerten, C. W. M. van der Geld, and B. J. Geurts, "Turbulence modification and heat transfer enhancement by inertial particles in turbulent channel flow," *Phys. Fluids* **23**, 123301 (2011).
- ² E. Russo, J. G. M. Kuerten, C. W. M. van der Geld, and B. J. Geurts, "Water droplet condensation and evaporation in turbulent channel flow," *J. Fluid Mech.* **749**, 666-700 (2014).
- ³ S. Elghobashi, "On predicting particle-laden turbulent flows," *Appl. Sci. Res.* **52**, 309-329 (1994).
- ⁴ A. Bukhovstova, E. Russo, J. G. M. Kuerten, and B. J. Geurts, "Comparison of DNS of compressible and incompressible turbulent droplet-laden heated channel flow with phase transition," *Int. J. Multiphase Flow* **63**, 68-81 (2014).
- ⁵ R. B. Bird, W. E. Stewart, and E. N. Lightfoot, *Transport Phenomena* (John Wiley and Sons, New York, 1960).
- ⁶ S. Sundaram and L. R. Collins, "Collision statistics in an isotropic particle-laden turbulent suspension. Part I. Direct numerical simulations," *J. Fluid Mech.* **335**, 75-109 (1997).
- ⁷ M. Chen, K. Kontomaris, and J. B. McLaughlin, "Direct numerical simulation of droplet collisions in a turbulent channel flow. Part I: Collision algorithm," *Int. J. Multiphase Flow* **24**, 1079-1103 (1998).
- ⁸ M. Chen, K. Kontomaris, and J. B. McLaughlin, "Direct numerical simulation of droplet collisions in a turbulent channel flow. Part II: Collision rates," *Int. J. Multiphase Flow* **24**, 1105-1138 (1998).
- ⁹ Y. Li, J. B. McLaughlin, K. Kontomaris, and L. Portela, "Numerical simulation of particle-laden turbulent channel flow," *Phys. Fluids* **13**, 2957-2967 (2001).
- ¹⁰ Y. Yamamoto, M. Pothoff, T. Tanaka, T. Kajishima, and Y. Tsuji, "Large-eddy simulation of turbulent gas-particle flow in a vertical channel: Effect of considering inter-particle collisions," *J. Fluid Mech.* **442**, 303-334 (2001).
- ¹¹ A. W. Vreman, "Turbulence characteristics of particle-laden pipe flow," *J. Fluid Mech.* **584**, 235-279 (2007).
- ¹² A. W. Vreman, B. J. Geurts, N. G. Deen, J. A. M. Kuipers, and J. G. M. Kuerten, "Two- and four-way coupled Euler-Lagrangian large-eddy simulation of turbulent particle-laden channel flow," *Flow, Turbul. Combust.* **82**, 47-71 (2009).
- ¹³ B. P. B. Hoomans, J. A. M. Kuipers, W. J. Briels, and W. P. M. van Swaaij, "Discrete particle simulation of bubble and slug formation in a two-dimensional gas-fluidized bed: A hard-sphere approach," *Chem. Eng. Sci.* **51**, 99-118 (1996).
- ¹⁴ H. Nasr, G. Ahmadi, and J. B. McLaughlin, "A DNS study of effects of particle-particle collisions and two-way coupling on particle deposition and phasic fluctuations," *J. Fluid Mech.* **640**, 507-536 (2009).
- ¹⁵ M. Breuer and M. Alletto, "Efficient simulation of particle-laden turbulent flows with high mass loadings using LES," *Int. J. Heat Fluid Flow* **35**, 2-12 (2012).
- ¹⁶ M. Sommerfeld, "The importance of inter-particle collisions in horizontal gas-solid channel flows," in *Gas-Particle Flows* (ASME FED, 1995), Vol. 228, pp. 335-345.
- ¹⁷ S. Yonemura, T. Tanaka, and Y. Tsuji, "Cluster formation in gas-solid flow predicted by the DSMC method," in *Gas-Solid Flows* (ASME FED, 1993), Vol. 166, pp. 303-309.
- ¹⁸ P. R. Brazier-Smith, S. G. Jennings, and J. Latham, "The interaction of falling water drops: Coalescence," *Proc. R. Soc. London, Ser. A* **326**, 393-408 (1972).
- ¹⁹ M. Orme, "Experiments on droplet collisions, bounce, coalescence and disruption," *Prog. Energy Combust. Sci.* **23**, 65-79 (1997).
- ²⁰ J.-P. Estrade, H. Carentz, G. Lavergne, and Y. Biscos, "Experimental investigation of dynamic binary collision of ethanol droplets—A model for droplet coalescence and bouncing," *Int. J. Heat Fluid Flow* **20**, 486-491 (1999).
- ²¹ D. Richard, C. Clanet, and D. Quéré, "Surface phenomena: Contact time of a bouncing drop," *Nature* **417**, 811 (2002).
- ²² M. A. van der Hoef, M. van Sint Annaland, N. G. Deen, and J. A. M. Kuipers, "Numerical simulation of dense gas-solid fluidized beds: A multiscale modeling strategy," *Annu. Rev. Fluid Mech.* **40**, 47-70 (2008).
- ²³ N. G. Deen, M. van Sint Annaland, M. A. van der Hoef, and J. A. M. Kuipers, "Review of discrete particle modeling of fluidized beds," *Chem. Eng. Sci.* **62**, 28-44 (2007).
- ²⁴ S. R. Turns, *Thermal-Fluid Sciences: An Integrated Approach* (Cambridge University Press, 2006).
- ²⁵ H. A. Stone, "Dynamics of drop deformation and breakup in viscous fluids," *Annu. Rev. Fluid Mech.* **26**, 65-102 (1994).
- ²⁶ R. Clift, J. R. Grace, and M. E. Weber, *Bubbles, Drops, and Particles* (Academic Press, 1978).
- ²⁷ C. Antoine, "Tension des vapeurs: Nouvelle relation entre les tension et les temperatures," *C. R.* **107**, 681-684 (1888).
- ²⁸ J. G. M. Kuerten, "Subgrid modeling in particle-laden channel flow," *Phys. Fluids* **18**, 025108 (2006).
- ²⁹ L. Kleiser and U. Schumann, "Treatment of incompressibility and boundary conditions in 3-D numerical spectral simulations of plane channel flows," in *Proceedings of the Third GAMM-Conference on Numerical Methods in Fluid Mechanics*, edited by E. H. Hirschel (Vieweg, Braunschweig, 1980), pp. 165-173.
- ³⁰ C. Marchioli, A. Soldati, J. G. M. Kuerten, B. Arcen, A. Tanière, G. Goldensohn, K. D. Squires, M. F. Cargnelutti, and L. M. Portela, "Statistics of particle dispersion in direct numerical simulations of wall-bounded turbulence: Results of an international collaborative benchmark test," *Int. J. Multiphase Flow* **34**, 879-893 (2008).
- ³¹ A. W. Vreman and J. G. M. Kuerten, "Comparison of direct numerical simulation databases of turbulent channel flow at $Re_\tau = 180$," *Phys. Fluids* **26**, 015102 (2014).
- ³² A. W. Vreman and J. G. M. Kuerten, "Statistics of spatial derivatives of velocity and pressure in turbulent channel flow," *Phys. Fluids* **26**, 085103 (2014).
- ³³ M. W. Reeks, "The transport of discrete particles in inhomogeneous turbulence," *J. Aerosol Sci.* **14**, 729-739 (1983).
- ³⁴ J. Young and A. Leeming, "A theory of particle deposition in turbulent pipe flow," *J. Fluid Mech.* **340**, 129-159 (1997).
- ³⁵ G. H. Ko and H. S. Ryou, "Modeling of droplet collision-induced breakup process," *Int. J. Multiphase Flow* **31**, 723-738 (2005).
- ³⁶ P. J. O'Rourke, "Collective drop effects on vaporizing liquid sprays," Ph.D. thesis (Mechanical and Aerospace Engineering, Princeton University, 1981).